Methane on a Stepped Surface: Dynamical Insights on the Dissociation of CHD$_3$ on Pt(111) and Pt(211)

Davide Migliorini[1], Helen Chadwick[1] and Geert-Jan Kroes[1,a]

[1] Leiden Institute of Chemistry, Gorlaeus Laboratories, Leiden University, P.O. Box 9502, 2300 RA Leiden, The Netherlands

ABSTRACT

The simulation of the dissociation of molecules on metal surfaces is a cornerstone for the understanding of heterogeneously catalyzed processes. However, due to high computational demand, the accurate dynamical simulation of the dissociative chemisorption of polyatomic molecules has been limited mostly to flat low-index metal surfaces. The study of surfaces that feature "defected" sites, such as steps, is crucial to improve the understanding of the overall catalytic process due to the high reactivity of under-coordinated sites for this kind of reaction. In this work we have extensively analyzed more than 10000 AIMD trajectories where a CHD$_3$ molecule is impinging either on the flat Pt(111) or on the stepped Pt(211) surface for different initial rovibrational states and collision energies. The results have been compared in order to get insights into the effect of the step in the dissociation of methane. We have found that, despite a large difference in the activation barrier and consequently in reactivity, the geometry of the lowest transition states is very similar on the two surfaces and this results in a similar dissociation dynamics. Furthermore, the trapping observed on the Pt(211) surface can be explained with energy transfer to parallel translational motion induced by the geometry of the slab and by a larger energy transfer to phonons for the stepped Pt(211) surface.

a) Email: g.j.kroes@chem.leidenuniv.nl

I. INTRODUCTION

The dissociative chemisorption of methane on a transition metal surface has been employed, both theoretically[1–10] and experimentally[11–14], as a model system to understand one of the most important steps in steam reforming[15], a fundamental industrial process which is currently one of the most common ways to produce molecular hydrogen. The CH bond cleavage on a Ni or Pt based catalyst is believed to be one of the rate determining steps[15] of the overall process in the high temperature regime. Due to the large complexity of molecule-surface reactions and to the necessity of treating accurately both the molecule and the metal slab, these systems have always been challenging for appropriate dynamical simulations[16–21]. The large number of degrees of freedom (DOFs) makes density functional theory (DFT) at the generalized gradient approximation (GGA) or meta-GGA level the go-to method for these systems and excludes any higher level of theory, at least for dynamical simulations[22]. Unfortunately, standard GGA and meta-GGA functionals are known for their poor accuracy in the calculation of activation barriers (E_b)[22] for molecule-surface systems; this has encouraged, in the last few decades, the pursuit of semi-empirical functionals[3,5,23–25] able to compute activation barriers with errors as small as 1 kcal/mol (~4.2kJ/mol), so-called chemical accuracy.

One of the viable semi-empirical methods to develop an accurate density functional is a variation of the specific reaction parameter (SRP) approach originally proposed by Truhlar and coworkers[26]. In our implementation for molecules on metals this approach consists of mixing two GGA functionals through a mixing parameter x so that the SRP functional is able to reproduce the experimental zero-coverage reaction probability (S$_0$) with chemical accuracy. This has been applied successfully to different catalytically relevant systems where a molecule dissociates on a low-index flat metal surface[3,5,23–25].

2

Recently, chemical accuracy has been achieved for CHD_3 on $Ni(111)$[5] using the SRP32-vdW functional

obtained by mixing the RPBE[27] and the PBE[28,29] exchange functionals (E_X^{RPBE} and E_X^{PBE}, respectively)

with a mixing parameter $x = 0.32$ together with the correlation functional developed by Dion $et\ al.$[30,31]

(E_C^{vdW-DF}) that also models van der Waal interactions. The SRP32-vdW functional reads as:

$$SRP32\text{-}vdW = 0.32 \cdot E_X^{RPBE} + (1 - 0.32) \cdot E_X^{PBE} + E_C^{vdw-DF}. \qquad (1)$$

The SRP32-vdW has been successfully transferred from CHD_3 dissociation on $Ni(111)$ to $Pt(111)$ and,

more importantly, it was able to achieve chemical accuracy also on the stepped $Pt(211)$ surface[3]. The

transferability of the SRP functional from the flat $Pt(111)$ to the stepped $Pt(211)$ surface suggests that an

SRP functional developed for a relatively simple system, such as the flat (111) surface, can be used to

obtain accurate reaction barriers on different defected sites of the same metal (see Ref. 3 and

references therein). The study of a stepped transition metal surface such as $Pt(211)$ is highly relevant for

heterogeneous catalysis since it is known that under-coordinated sites usually show enhanced reactivity

for processes like the dissociative chemisorption of methane[32–36]. Moreover the dissociation of methane

on $Pt(211)$ has been previously used to model the overall catalytic process through microkinetic

simulations[1,2].

In this work we have analyzed 12500 $ab\text{-}initio$ molecular dynamics (AIMD) trajectories of CHD_3 impinging

on both $Pt(111)$ and $Pt(211)$ in order to study and compare the dynamical features of the dissociation on

the two surfaces focusing on the differences introduced by the presence of the step. The paper is

organized as follows: the method used to set up, propagate and analyze the trajectories is reported in

Section II, the results are presented and discussed in Section III and the main conclusions are

summarized in Section IV.

II. METHOD

Most of the results discussed in this paper have been obtained by analyzing AIMD trajectories of CHD_3 impinging on the Pt(111) and on the Pt(211) surfaces. These simulations have been used to compute the zero-coverage reaction probability (S_0) which has been compared to molecular beam experiments to define and test the SRP32-vdW functional for said systems[3]. The computational details have been extensively discussed in recently published work[3] and therefore they will only be summarized in this section.

The electronic structure calculations have been performed on a DFT level using the Vienna *Ab Initio* Simulation Package (VASP)[37–40] version 5.3.5. The first Brillouin zone has been sampled with a 4x4x1 Γ-centered k-point grid and the basis set includes plane waves with kinetic energy up to 350 eV. The core electrons have been represented through projector augmented-wave (PAW) pseudopotentials[41,42]. The Pt(111) surface has been represented using a 5 layers (3x3) supercell slab, consistent with previous work[3,6]. The stepped Pt(211) surface has been modelled using a 4 layer (1x3) supercell. For both surfaces, the slab is separated from its first periodic replica by 13 Å of vacuum. A 0.1 eV Fermi smearing has been used to facilitate the SCF convergence. The set up used for these calculations has been extensively tested and the results of the tests are available in the Supporting Information of Ref. 3.

The AIMD trajectories have been set up in order to reproduce the molecular beam experiments performed by Beck and co-workers[3] including the surface temperature (T_S) of 500 K and 650 K for Pt(111) and Pt(211) respectively, and modelling the initial kinetic energy and ro-vibrational population of the methane molecules. Note that, even though the simulations have been performed at different temperatures for the two surfaces, previous work suggests that the temperature dependence of the reactivity on Pt is small[6,43]. Quasi-classical trajectories (i.e., classical trajectories where the vibrational

zero-point energy is imparted to the molecule) have been propagated with a 0.4 fs time-step until

dissociation or scattering was observed. A molecule has been considered reacted if a bond was

stretched over 3.0 Å and it has been considered scattered if, after the impact, it reached a certain

distance above the surface (i.e., 6.0 Å or 6.5 Å for Pt(111) and Pt(211), respectively) while the center of

mass (COM) velocity was pointing away from the surface. For the reactive trajectories the time of the

dissociation (t_{diss}) has been defined as the first time step at which the dissociating bond is as elongated

as in the minimum energy transition state ± 0.04 Å. In this work the molecules that did not reach an

outcome within the first 2 ps of propagation have been considered trapped.

The transition state (TS) geometries presented have been computed using the dimer method included in

the VASP Transition State Tools package (VTST)[44–47]. Frequency analysis calculations have been

performed to confirm that all the TSs reported in this work are true 1st order saddle points (i.e., one and

only one imaginary frequency is present) except where stated differently.

The analysis has been carried out on 7000 trajectories for Pt(111) and on 5500 trajectories for Pt(211)

for an initial average incident energy ($\langle E_i \rangle$) ranging between 60.7 and 120.1 kJ/mol for Pt(111) and

between 58.2 and 107.9 kJ/mol for Pt(211). Several dynamics-relevant features have been investigated

and the results have been binned and smeared using a sum of Gaussian curves such that, for a sample of

N data, the final distribution $\mathcal{F}(\alpha)$ of the observable α is represented as:

$$\mathcal{F}(\alpha) = \sum_i^{Nbins} \sum_j^{Ndata} \frac{1}{\sqrt{2\pi\sigma_G{}^2}} \cdot exp\left(-\frac{(bin_0 + i * binsize - data(j))^2}{2\sigma_G{}^2}\right) \quad\quad (2)$$

where the indices i and j run over the bins and the data respectively, bin_0 is the first value of α

considered for the binning procedure and σ_G is the standard deviation of the Gaussian used (i.e., the

broadening). The final distribution is the sum of Gaussians centered on the data values for each element

of the dataset. Since we are comparing datasets of different sizes the area of the final distributions is

always normalized to 1. Distributions reported in the same plot always have the same broadening σ_G

and all the distribution parameters are reported in the Supplementary Material (SM).

Using a broadening can improve the quality and the readability of the results but can cause small tails at

the edge of the distribution that might assume unphysical values. However this does not affect the

interpretation of the results. In order to calculate the distributions all the available trajectories have

been used. This means that the distribution takes into account results for different CHD_3 vibrational

states and average collision energies (see Ref. 3) unless explicitly stated. For some of the observables α

the average value is reported together with the standard deviation σ and standard error σ_M.

$$\sigma = \sqrt{\frac{\sum_{i=1}^{N}(\alpha_i - \langle\alpha\rangle)^2}{N-1}} \tag{3}$$

$$\sigma_M = \frac{\sigma}{\sqrt{N}} \tag{4}$$

Here, N is the sample size and $\langle\alpha\rangle$ is the sample average.

III.   RESULTS AND DISCUSSION

Platinum is an fcc metal and its (111) surface shows the well-known hexagonal lattice structure. The

Pt(211) surface is composed of a 3 atoms wide (111)-like terrace and a (100)-like step. In order to

analyze the dynamics on the Pt(211) three non-equivalent sites have been defined: edge (on the step

edge), middle (the row of atoms in the middle of the terrace) and bottom (the row of atoms on the low

end of the step). Moreover some of the analysis is referenced to facets instead of sites considering the step (i.e., the (100) facet) and the terrace (i.e., the (111) facet). The side and top views of the surfaces are shown in Fig. 1 where the atoms are reported in their equilibrium positions and the step facet is highlighted in green for the Pt(211) surface. The impact (reaction) site is defined as the nearest site (i.e., bottom, middle or edge) in the xy plane at the closest approach (reaction) time. Molecules that hit the surface or dissociate at an x coordinate between the edge and the bottom site (green shaded area in Fig. 1) are considered step facet events. It has been shown in previous work[3] that the reactivity on the stepped surface happens almost completely through the dissociation on top of the step edge atom. Therefore the analysis of reacted trajectories has been carried out by looking at the different behavior of molecules impacting on the different surface sites (i.e., edge, middle and bottom atoms). For non-reactive trajectories the differences in the dynamics upon impacting on the (111)-like terrace facet or on the (100)-like step facet have also been considered.

On the Pt(211) surface trapping has been observed and the average trapping time has been estimated to be about 40 ps[3] (i.e., 43 ps), which is too short to be detected experimentally and too long to be simulated with an expensive method like AIMD. For the previously published work the trapped trajectories have been propagated for 1 ps (or 2 ps in a few test cases). Therefore, to ensure a fair analysis, in this work all the trapped trajectories have been propagated up to 2 ps. Out of the 69 trajectories that were trapped after 1 ps 35 have scattered upon further propagation. However this does not necessarily affect the main conclusions of earlier work since a large number of trapped trajectories are still present even after 2 ps of propagation, especially at low incidence energy. This also suggests that, in order to be trapped (i.e., characterized by some average trapping time), the molecules need some time to equilibrate with the surface.

To understand the dynamics of the CHD_3 on the different surfaces, the number of bounces has been counted for all the trajectories, where a bounce is defined as two sign-changes of the COM velocity

along the direction parallel to the macroscopic surface normal (z). As observed for other metal surfaces, the CHD_3 dissociative chemisorption is usually a "sudden" process: on both platinum surfaces the molecules react on the first impact and without bouncing. This is also true for almost all the scattered trajectories on Pt(111) (only 5 out of more than 6500 perform one and only one bounce) and for most of the scattered trajectories on Pt(211). On Pt(211) (see Fig. 2) we observe few trajectories bouncing either one or two times before scattering and that the trapped trajectories bounce between one and four times during the propagation.

A. Transition States

Several transition states have been located on the stepped Pt(211) surface by performing calculations using the dimer method[44–47]. All the TSs presented are real 1st order saddle points as confirmed by a normal mode analysis unless stated differently. The energy (i.e. the barrier height, E_b), the length of the dissociating CH bond (r) and the θ, β and γ angles have been determined. θ is the angle between the dissociating bond and the surface normal (i.e., z) and β is the angle between the umbrella axis ($\vec{a}$) and the surface normal, where $\vec{a}$ is defined as the vector going from the geometric center of the umbrella hydrogens to the carbon atom (Fig. 3). γ is the angle between the dissociating CH bond and the $\vec{a}$ axis. The γ angle describes the internal geometry of the TS while β and θ describe the geometry of the molecule with respect to the macroscopic surface normal. All the results, compared to the minimum energy TS for the flat Pt(111) surface, are reported in Table I including all the TS geometries (also represented in Fig. 4) and the studied angles (also shown in Fig. 3). The angle α (sketched in Fig. 3 and reported in Table I) describes the orientation of the dissociating bond in the xy plane for the Pt(211) surface and it will be discussed later in this paper.

Table I. Comparison of the TSs found on the two platinum surfaces. For each TS is reported: the surface on which it has been found, the Label as in Fig. 4, the name of the TS, the θ, β, γ and α angles, the length of the dissociating bond (r) in Å and the energy barrier (E_b) in kJ/mol. Note that if the energy barrier is followed by a star (*) the TS reported still has a second imaginary frequency (i.e., it is not a real 1st order saddle-point).

Surface	Label	Name	θ [˚]	β [˚]	γ [˚]	α [˚]	r [Å]	E_b [kJ/mol]
Pt(111)	A	-	133.4	168.3	34.8	-	1.55	78.6
Pt(211)	B	Edge2Edge-B1	132.9	166.0	33.1	85.0	1.53	53.9
Pt(211)	C	Edge2Mid-H2	115.6	145.6	30.0	181.3	1.60	57.1
Pt(211)	D	Edge2Mid-H1	113.7	145.9	32.2	179.4	1.62	57.7 *
Pt(211)	E	Edge2Bot-B1	122.9	156.8	33.9	0.5	1.65	65.1 *
Pt(211)	F	Mid2Bot-B1	145.8	171.8	35.0	226.3	1.55	97.9
Pt(211)	G	Mid2Mid-B1	130.2	158.5	34.9	72.1	1.57	98.0
Pt(211)	H	Mid2Edge-B1	119.0	151.7	33.4	25.3	1.56	96.4

For Pt(211), four TSs have been found on top of a step edge atom, with a different orientation of the dissociating CH bond. These have been labeled according to the positions of the carbon and of the dissociating hydrogen: Edge2Edge-Bridge (Edge2Edge-B) dissociating parallel to the step edge (Fig. 4B), Edge2Middle-Hollow (Edge2Mid-H) dissociating on a hollow site towards the middle row of the terrace (Figs. 4C and 4D) and Edge2Bottom-Bridge (Edge2Bot-B) dissociating towards a bridge site on the (100) step site (Fig. 4E). Note that the two TS depicted in Fig. 4C and 4D are related by a hindered rotation about the umbrella axis. Three TSs have been found on the middle terrace atom dissociating towards different bridge sites and they have been labeled as Middle2Bottom-Bridge (Mid2Bot-B), Middle2Middle-Bridge (Mid2Mid-B) and Middle2Edge-Bridge (Mid2Edge-B) according to which site they are dissociating towards (Figs. 4F, 4G and 4H, respectively). The numbers, either 1 or 2, at the end of a TS name identify the eclipsed or the staggered orientation of the umbrella relative to the dissociating CH bond, respectively. Note that the TSs depicted in Figs. 4D and 4E still have a second small imaginary frequency (i.e., they are not real 1st order saddle points. See Table I).

There is a clear difference in the E_b between the step edge atom and on the terrace middle atom (i.e., ≈ 39 kJ/mol on average) regardless of the molecular orientation: the TSs centered on the step edge atom

have very similar energies and the same is true for the TSs centered on the terrace middle atom. The step edge site is more reactive than the flat Pt(111) surface while terrace middle sites show barriers even larger than on the ideal flat surface (78.6 kJ/mol, Table I). Despite this large range of E_b the TSs are geometrically similar: all of them have a dissociating bond length between 1.53 and 1.65 Å and an angle γ between the dissociating bond and $\vec{a}$ between 30 and 35˚. As expected β and θ show more variability because they depend on the molecular geometry as well as on the surface orientation with respect to the reference frame (z axis). β and θ can be compared for the TS on Pt(111) and the lowest energy TS on Pt(211) (i.e., Edge2Edge-B1) and, for both the angles, they have the same values within less than 2.5˚.

B. Energy Transfer to Parallel Motion

In Fig. 5 the COM lateral displacement (δ_{COM}) has been reported for all the trajectories, where δ_{COM} has been computed as the difference between the COM xy position at the initial and at the reaction step (for dissociative events) or at the step of 1st closest approach (for scattered and trapped trajectories). For the flat surface the reactive events happen in a "sudden" fashion where the molecule does not change its position in the xy plane significantly, as they show $\langle \delta_{COM} \rangle$ smaller than 0.09 Å (Fig. 5A). The same is true for the molecules reacting on the step edge of Pt(211) (Fig. 5B). Scattered and trapped molecules on Pt(211) show a significantly larger $\langle \delta_{COM} \rangle$ that can go up to 0.25 Å for molecules trapped after impacting on the step facet (all the data are reported in the SM). This is due to the fact that, even though all molecules start with a COM velocity aligned with the z axis, the topology of the surface can induce energy transfer from the translational motion in the z direction to the motion along the surface (energy transfer to parallel motion). In order to study this phenomenon, the distance travelled in the xy plane has been computed (for each individual trajectory) as:

$$d_{xy} = \sum_{t=1}^{T} \sqrt{(x_t - x_{t-1})^2 + (y_t - y_{t-1})^2}$$

(5)

$$d_{\alpha=x,y} = \sum_{t=1}^{T} |\alpha_t - \alpha_{t-1}|$$

(6)

Here, d_{xy} is the distance travelled in the xy plane and d_α is the distance travelled in the α direction (i.e., $\alpha = x, y$), and t is the time step. T is the total number of time steps. Note that d_{xy} and d_α are dependent on the time step (0.4 fs) and on the total propagation time (i.e., the number of time steps T). On Pt(211), x and y are perpendicular and parallel to the step edge, respectively. If we consider d_{xy}, reported in Fig. 6, it is noticeable how the molecules scattered from the step can travel significantly more than the ones scattered from the flat surface (Fig. 6A and 6B). On average we observe $\langle d_{xy} \rangle$ = 0.8 Å on Pt(111) and $\langle d_{xy} \rangle$ = 2.8 Å on Pt(211) but on the stepped surface scattered molecules have been observed to travel up to 30 Å.

If we look at the trajectories trapped on the Pt(211) surface (Fig. 6C) we can see that the molecules can travel considerable distances in our simulations (i.e., up to almost 50 Å) especially in the direction perpendicular to the step edge (i.e., along x). Note that for these trajectories the propagation has been stopped after 2 ps and the more we would propagate them the further they would travel. This is due to the large velocity the trapped molecules have in the xy plane.

The distribution of the average velocity in xy upon trapping ($\langle V_{xy} \rangle^{trap}$) is reported in Fig. 6D. $\langle V_{xy} \rangle^{trap}$ has been computed as:

$$\langle v_{xy} \rangle^{trap} = \sum_{t=1}^{N^{trap}} \frac{\sqrt{v_{x(t)}^2 + v_{y(t)}^2}}{N^{trap}} \tag{7}$$

$\langle V_{xy} \rangle^{trap}$ is averaged over the total of N^{trap} time steps. Here t ranges from the first impact with the surface to the last step of the propagation (i.e., when the molecule is considered trapped). The velocity distribution is centered on $\langle V_{xy} \rangle^{trap}$ = 0.014 Å/fs which means that during the estimated trapping time of 43 ps, those molecules can travel, on average, as far as 593 Å and this goes up to 642 Å if we consider only the molecules trapped after impinging on the step. This suggests that the trapped molecules have enough time to explore a large portion of the surface, increasing their chance of finding a favorable orientation to react or even a higher order defect with a lower dissociation barrier, such as kinks.

The importance of the energy transfer from motion normal to the surface to motion parallel to the surface can be quantified by calculating the amount of kinetic energy that molecules have in the xy plane after the impact with the surface (K_{xy}). To ensure a fair comparison, K_{xy} has been calculated at the end of the trajectory for scattered molecules and at the first outer turning point for trapped molecules. In Fig. 7 K_{xy} is reported for scattered and trapped molecules on Pt(211) distinguishing between molecules which impact on the step facet and on the terrace facet. As expected both trapped and scattered molecules show large values of K_{xy}. Moreover, the step site is more efficient than the terrace in promoting energy transfer to the parallel motion, probably because it makes a larger angle with the normal to the macroscopic surface. In Fig. 8 $\langle K_{xy} \rangle$ is reported as a function of the initial average collision energy of the molecules ($\langle E_i \rangle$). The energy transfer to parallel translational motion increases with $\langle E_i \rangle$ and confirms that the step induces more energy transfer to the parallel motion than the terrace. The values of $\langle K_{xy} \rangle$ for the trapped trajectories show large error bars due to the small sample

12

size but the results suggest that the trapped molecules show a larger energy transfer to the parallel motion than the scattered ones at low $\langle E_i \rangle$ (Fig. 8). In turn, this suggests that, especially at low $\langle E_i \rangle$, energy transfer to parallel motion at the step contributes to the trapping.

Out of a total of 34 trapped trajectories 25 of them impacted on the step while only 9 on the terrace. If we weight these results according to the step:terrace area ratio (i.e., 1:1.8) we find that the trapping probability is 5 times larger if the molecule impacts on the step than on the terrace. The xz projection of the first part of the trapped trajectories is reported in Fig. 9. In Fig. 10 is reported the distribution of the average velocity in x for the trapped molecules ($\langle v_x \rangle^{trap}$). Again, these results suggest that one of the main reasons for the trapping we observe on Pt(211) is due to the geometry of the surface: the molecules that hit the step undergo energy transfer to parallel translational motion and start travelling in the positive x direction. Most of the molecules impacting on the terrace travel in the negative x direction.

C. Energy Transfer to Surface Phonons

The energy transfer from the molecules to the surface phonons (E_T) is reported in Fig. 11. All the scattered molecules transfer roughly the same amount of energy to the phonons independently from the Pt surface on which they impact; on average molecules that hit the Pt(111) and the Pt(211) surface show $\langle E_T \rangle$ = 15.5 ± 0.2 and 13.9 ± 0.2 kJ/mol respectively. Note that Pt(111) shows a somewhat larger $\langle E_T \rangle$ but the AIMD trajectories have been performed over a larger range of $\langle E_i \rangle$. This can be seen in Fig. 11B where E_T is reported as a function of the incident energy: the linear regression for the two sets of data show the same slope (i.e., 0.165) and very similar intercepts (i.e., 0.914 kJ/mol and 1.400 kJ/mol for Pt(111) and Pt(211), respectively). Note that the difference of 0.486 kJ/mol in the intercept is smaller than the average error for both surfaces (i.e., 0.527 kJ/mol and 0.514 kJ/mol for Pt(111) and Pt(211),

13

respectively). The small number of trapped trajectories reduces the statistical significance of their analysis. However the results suggest that, especially at low $\langle E_i \rangle$, some trajectories can undergo a larger energy transfer to the surface phonons (i.e., $\langle E_T \rangle$ = 23.2 ± 1.9 kJ/mol) which would increase the probability of being trapped. This suggests that energy transfer to the phonons contributes to the trapping on Pt(211).

The E_T has been calculated approximately from the molecular kinetic (K) and potential (V) energy. The initial configuration (i) is always the first step of the dynamics. For the scattered molecule, the final configuration (f) is taken from the last step of the dynamics while for the trapped molecule we considered the E_T upon first impact with the surface and therefore the final configuration is taken from the first outer turning point configuration. This means that, in the initial and in the final configurations, the molecules might not be at the same distance from the slab. Therefore the energy transfer has been estimated using Eq. 8a, which includes a correction for the interaction energy (I). I has been computed using Eq. 8b and subtracting the absolute energy of the isolated CHD_3 and of the bare slab from the energy of the system containing both the molecule and the metal surface.

$$E_T = -\left[\left(K_f + V_f + I_f \right) - \left(K_i + V_i + I_i \right) \right] \tag{8a}$$

$$I = V_{slab+CHD3} - V_{slab} - V_{CHD3} \tag{8b}$$

D. Reaction Site and Dissociation Geometry

On Pt(211) the vast majority of the reactive events happen on the step edge. The reaction site has been studied by measuring the distance in the xy plane from the center of mass of the molecule to the closest atom in the first layer and reporting the distributions for all the trajectories simulated. Results

are reported in Fig. 12A for Pt(111) and in Fig. 12B for Pt(211) for the reacted molecule at t=0 and at the time of the dissociation (t=t_{diss}). For both surfaces the reaction happens preferentially close to top sites (i.e., atoms in the first layer) but for the stepped surface a considerable number of molecules dissociates further than 1 Å away from the closest Pt atom.

The effect of the orientation of the molecules on reaction has been analyzed by monitoring the β (Fig. 13), the θ (Fig. 14) and the γ (Fig. 15) angles throughout the dynamics and investigating their dependence on $\langle E_i \rangle$ (Fig. 16). These three angles describe the orientation of the umbrella axis (β) and of the dissociating bond (θ) with respect to the surface normal and the angle between the dissociating bond and the umbrella axis (γ) (see Fig. 3). The angles have been computed at the start of the trajectories (t=0) and at the time of the dissociation (t=t_{diss}) for the reactive trajectories. For both θ and β the initial distribution considering all the molecules simulated is a sine distribution proving the accurate random sampling of the initial conditions.

Comparing the Pt(111) to the Pt(211) results one can see that the dissociation dynamics on the two surfaces are qualitatively very similar: the two known key aspects of the dissociation of CHD_3 on Pt and Ni are the pre-orientation of the dissociating bond[4,5] and the umbrella reorientation[4]. The distributions of θ reported in Fig. 14 show that only bonds initially pointing towards the surface (i.e. close to the TS value of $\theta \approx 133°$) can dissociate and that the angular acceptance range for the dissociation on the Pt(211) surface is broader as the final θ distributions are less localized and exhibit larger σ values (see Fig. 14 and Table II). The results for β (see Fig. 13) confirm the important role of the umbrella reorientation[4] for CHD_3 on Pt(111), and extend this confirmation to the reaction on the stepped Pt(211) surface as well. In order to react, the molecule not only needs to approach the surface with the CH bond pre-oriented towards the surface, but in the meantime the umbrella has to swing upwards increasing the value of β. In previous work[4] Füchsel *et al.* studied the dissociation of CHD_3 on Pt(111) and, for $\langle E_i \rangle$ between 49 and 84 kJ/mol, they observed that the center of the distributions of θ do not shift during

the reaction. Extending the range of initial average kinetic energy we do observe a dependence of θ and

of γ on $\langle E_i \rangle$ at the time of the reaction (see Fig. 16) that can be explained by considering that, since the

hydrogen (or deuterium) atom is oriented towards the surface, the dissociating bond bends away from

the surface upon impacting on the slab proportionally to the COM velocity and thus results in a decrease

of θ and in an increase of γ (since β does not depend on $\langle E_i \rangle$).

Table II. Average value, standard deviation (σ) and standard error (σ_M) for β, θ and γ at the time of the dissociation as reported in Figs. 13, 14 and 15, respectively.

Surface	β [˚]		θ [˚]		γ [˚]	
	$\langle \beta \rangle \pm \sigma_M$	σ	$\langle \theta \rangle \pm \sigma_M$	σ	$\langle \gamma \rangle \pm \sigma_M$	σ
Pt(111)	149.9 ± 0.6	12.1	123.6 ± 0.5	10.2	33.8 ± 0.6	13.0
Pt(211)	141.2 ± 1.1	16.7	117.3 ± 1.0	15.0	31.9 ± 0.8	12.2

Fig. 16 also shows that, at the moment of the dissociation, β and θ (Figs. 16A and 16B) are smaller for

Pt(211) than for Pt(111) while γ is very similar (Fig. 16C). This suggests that at the moment of the

reaction the internal molecular geometry is the same on the two surfaces. However the molecules react,

on average, more parallel to the macroscopic surface for the stepped Pt(211). This can be explained by

looking at the θ angle of the TSs on the two surfaces. All the TSs on Pt(111) show $\theta \approx 133$˚ (see Table III in

Ref. 48) which is the same value of the lowest E_b TS on Pt(211) (Edge2Edge-B1 in Fig. 4B and Table I).

However, the TSs perpendicular to the step edge on Pt(211) (i.e., C, D and E in Table I) show values of θ

about 10-19˚ smaller and this effectively broadens the angular acceptance range for the dissociation on

the stepped surface. The TSs C, D and E dissociate in the direction perpendicular to the step edge and,

even though they show larger E_b, they play a big role in the dissociative process. In Fig. 17 the

distribution of the angle α is plotted at t=0 and the moment of the dissociation for molecule reacting on

the step edge atom. α is defined as the counter-clockwise angle between x and the projection of the

dissociating bond on the xy plane. Therefore, α=0˚ corresponds to a dissociation in the x direction and

α=90˚ corresponds to the y direction (i.e., perpendicular and parallel to the step edge, respectively).

Even though the minimum energy barrier TS occurs at $\alpha \approx 0°$ (and, equivalently, at $\alpha \approx 270°$), most of the reactions on the step edge atom happen for $\alpha \approx 180°$. This can be partially explained taking into account that the orientation of the molecules is sampled as $\sin(\theta)$ which makes $\theta \approx 114°$ (i.e., the ideal value for $\alpha = 180°$) oversampled with respect to $\theta \approx 133°$ (i.e., the ideal value for $\alpha = 90°$) (see Table I).

IV.   SUMMARY AND CONCLUSION

In this work we have analyzed a total of 12500 trajectories where CHD_3 is impinging either on the flat Pt(111) or on the stepped Pt(211) surface. Moreover several different TSs have been found on the Pt(211) surface. Despite all the TSs found having a very similar molecular geometry, the ones located on a step edge atom of the Pt(211) surface show a significantly lower energy barrier while the ones on the terrace middle atom have larger barrier heights, even larger than for the flat Pt(111) surface. On both surfaces the dissociation has been shown to proceed through a very similar mechanism where the dissociative CH bond needs to be pre-oriented towards the surface and the methyl umbrella rotates upwards to promote the reaction. However the stepped Pt(211) has a broader angular acceptance range for the dissociative chemisorption and the molecules react on average more parallel to the surface. The stepped Pt(211) surface can trap molecules due to a larger energy transfer to phonons and to geometry-promoted energy transfer to parallel translational motion. The large velocity in the direction parallel to the surface of the trapped trajectories suggests that they can travel long distances, on average more than 600 Å for step impacts with trapping times > 1 ps, while bouncing on the surface. This implies that, in experiments, the trapped molecule has time to explore the surface and therefore it has an increased probability of reacting by finding the most favorable geometry or even a higher order defect, such as kinks.

SUPPLEMENTARY MATERIAL

The Supplementary Material contains Tables with the averages, the standard deviations and the binning parameters for all the data reported in the paper.

ACKNOWLEDGMENTS
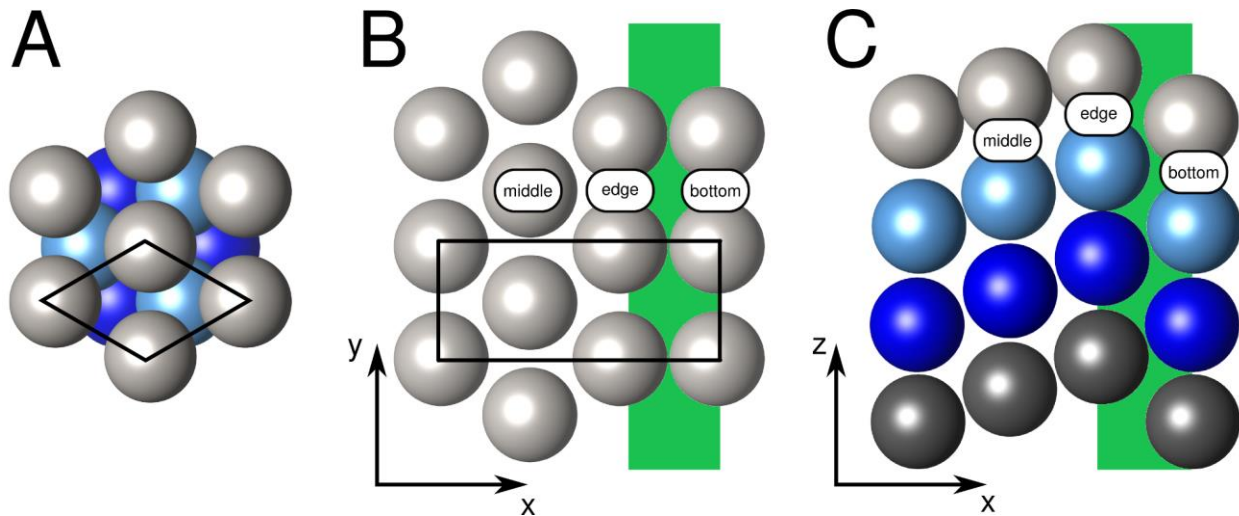
Figure 1. Panel A: top view of the Pt(111) surface. Panel B: top view of the first layer of the Pt(211) surface. Panel C: side view of the Pt(211) surface. For both the surfaces the atoms are reported in their equilibrium position. The unit cell is marked in black and different layers are reported in different colors. For the Pt(211) surface the three rows of atoms in the unit cell are called edge, middle and bottom according to their position: edge is on top of the step edge, middle is in the middle of the terrace, and bottom is on the low side of the step. The (100) step is shaded in green while the remainder of the surface is the (111) terrace.
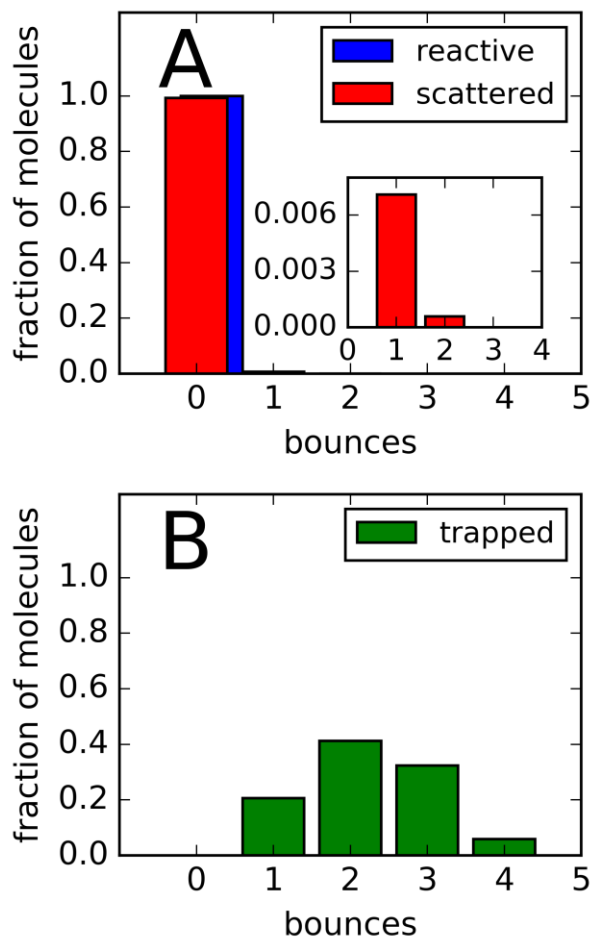
Figure 2. Number of bounces for the molecules impinging on the Pt(211) surface. Panel A reports in red and blue the fraction of scattered and reacted trajectories, respectively. The inset in Panel A is a magnification for the few trajectories that bounce before scattering. Panel B reports the results for the trapped trajectories on Pt(211).
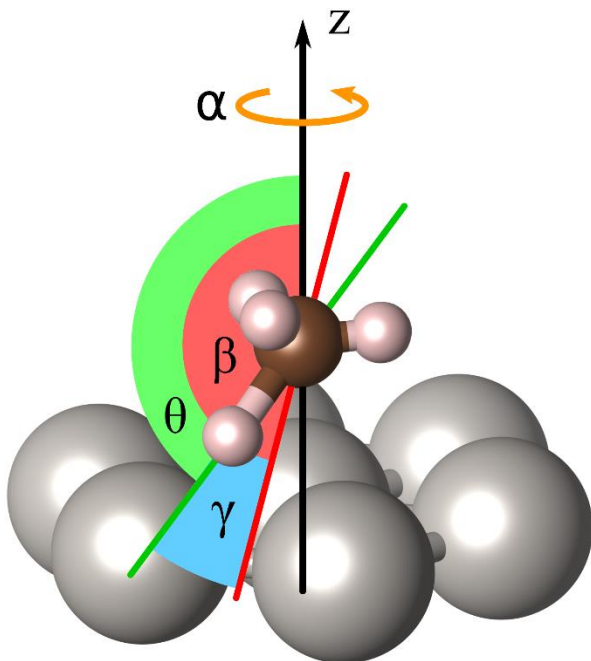
Figure 3. Sketch of the angles studied: θ (green shade) is the angle between the CH bond (green line) and the z axis, β (red) is the angle between the the umbrella axis $\vec{a}$ (red line) and the z axis (i.e., the macroscopic surface normal) and γ (blue) is the angle between the CH bond and the umbrella axis $\vec{a}$. The angle α (orange) represents the orientation of the dissociating bond in the xy plane.
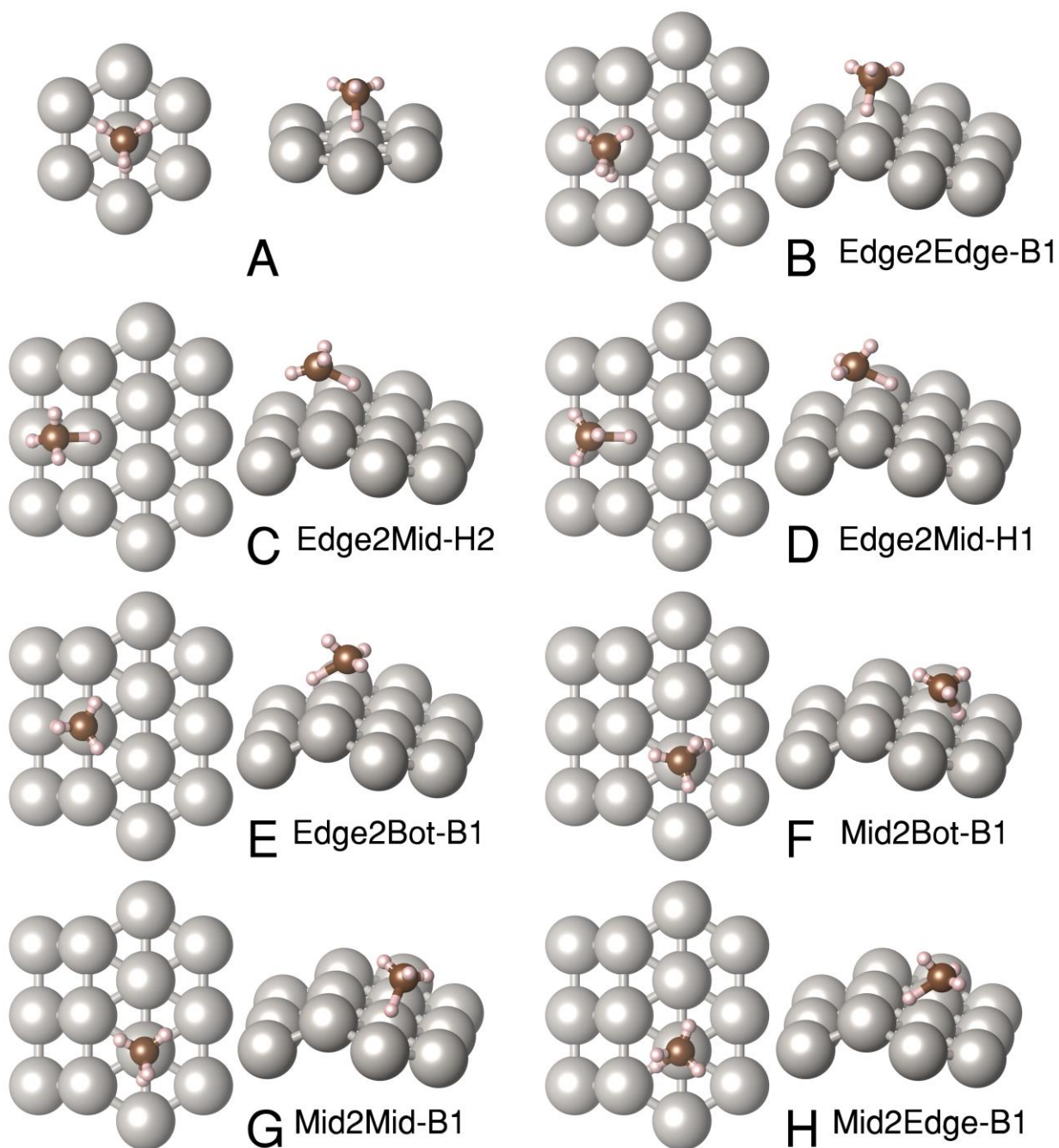
Figure 4. Depiction of the transition state geometries found in side and top view. TS A is the one found for Pt(111) and reported in Ref. 3. TSs B to H have been found on Pt(211) and are also labeled with the names reported in Table I.
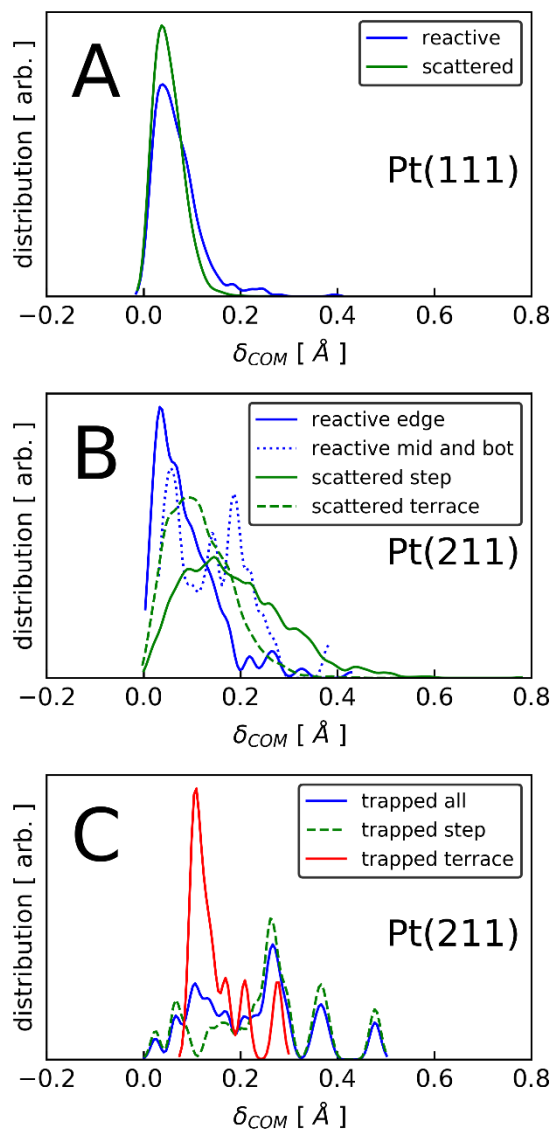
Figure 5. Panel A: δ_{COM} computed for the reactive (blue) and scattered (green) trajectories on Pt(111).

Panel B: δ_{COM} computed for the reacted (blue) and scattered (green) trajectories on Pt(211), the solid

lines describe step edge atom reaction and step facet scattering, the dotted line describes bottom and

middle atom reactions and the dashed line describes terrace facet scattering. Panel C: δ_{COM} computed

on Pt(211) for all the trapped trajectories (blue) and for the trapped trajectories impacting first on the

step (green) or on a terrace (red).
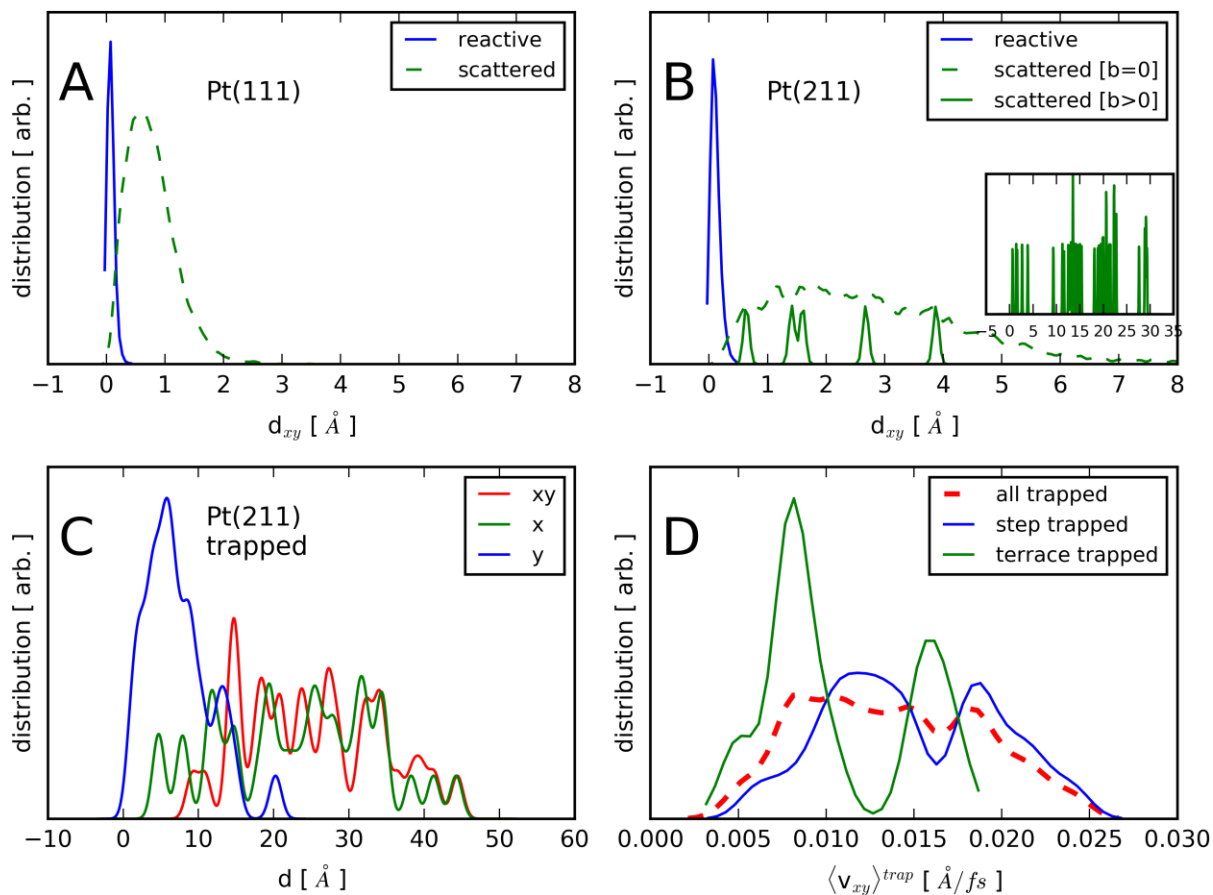
Figure 6. Panel A and B: distributions of the distance travelled by the molecules in the xy plane (d_{xy}) for reactive and scattered trajectories on the Pt(111) and Pt(211) surfaces, respectively. In Panels A and B the blue solid lines represent reactive trajectories (the distributions have been multiplied by 0.2 for a better comparison) and the green lines represent scattered trajectories without bouncing (b=0, dashed green) and with bouncing (b>0, solid green) on the surface. Panel C: distance travelled (d) by the molecules trapped on the Pt(211) surface. The distance travelled in the x direction, in the y direction and the total distance travelled in the xy plane are reported in green, blue and red respectively. Panel D: distribution of average COM velocity in the xy plane for the trapped trajectories $\langle v_{xy} \rangle^{trap}$ for molecules that have the first impact on the terrace (green solid line), on the step (blue solid line) and for all the trapped molecules (red dashed line).
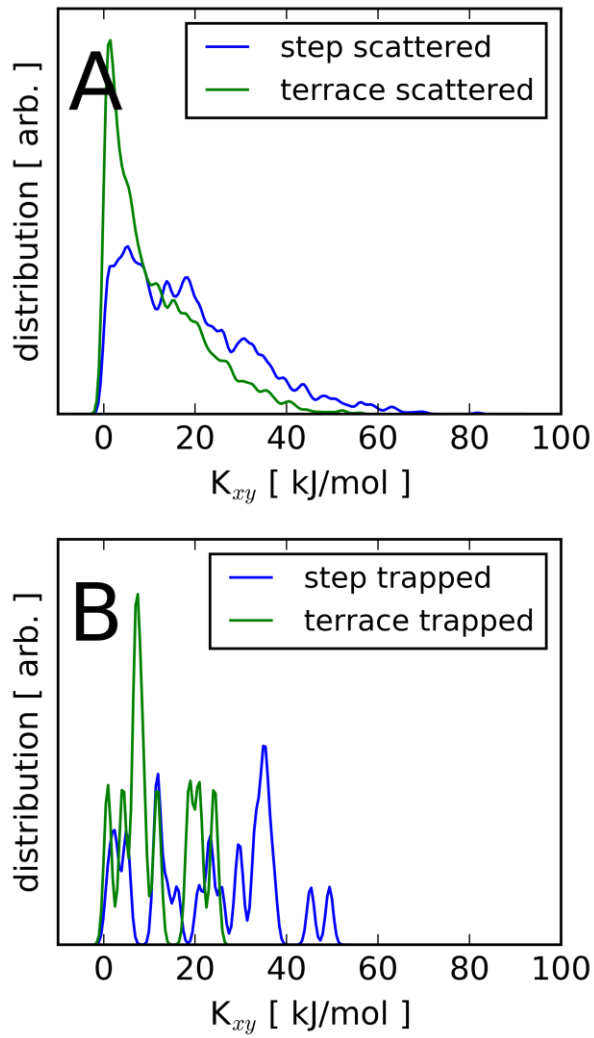
Figure 7. Distribution of kinetic energy in the xy plane (K_{xy}) after the impact with the Pt(211) surface for scattered and trapped molecules (Panel A and B, respectively) and for molecules that impacted on the step or on the terrace (blue and green, respectively).
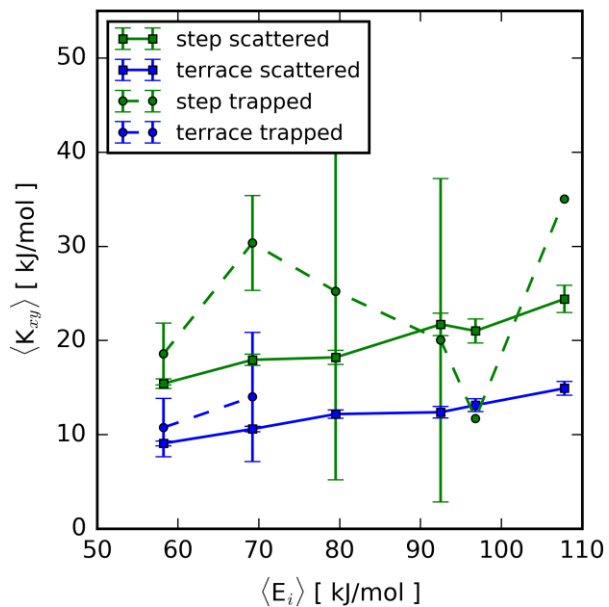
Figure 8. Average kinetic energy in the xy plane ($\langle K_{xy} \rangle$) as a function of the average initial kinetic energy ($\langle E_i \rangle$) after the impact with the Pt(211) surface. Results for scattered molecules are reported as squares and solid lines and results for trapped molecules as circles and dashed lines. Green data represent molecules impacting on the step and blue data molecules impacting on the terrace. Two points are reported without error bars because the sample size for those data sets is 1. The lines are drawn to guide the eye.
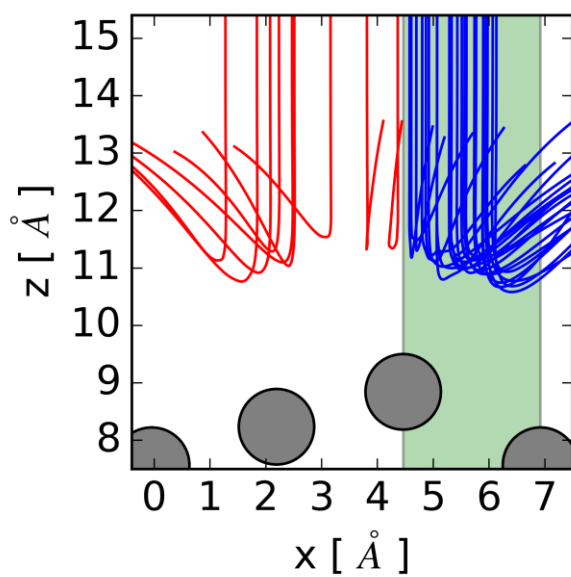
Figure 9. xz projection of the first part of the trapped trajectories. The first layer atoms 0 K positions are reported as gray circles and the step is highlighted in green. The trajectories are reported in blue if the first impact is on the step and in red if it is on the terrace.
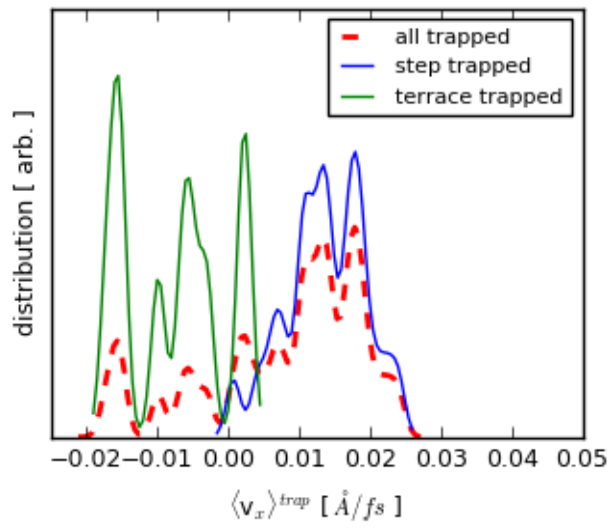
Figure 10. Distribution of the average velocity along x during trapping $\langle v_x \rangle^{trap}$ for all the trapped

molecules (red line), the trapped molecules that have the first impact on the step (blue) and the ones

that have the first impact on the terrace (green).
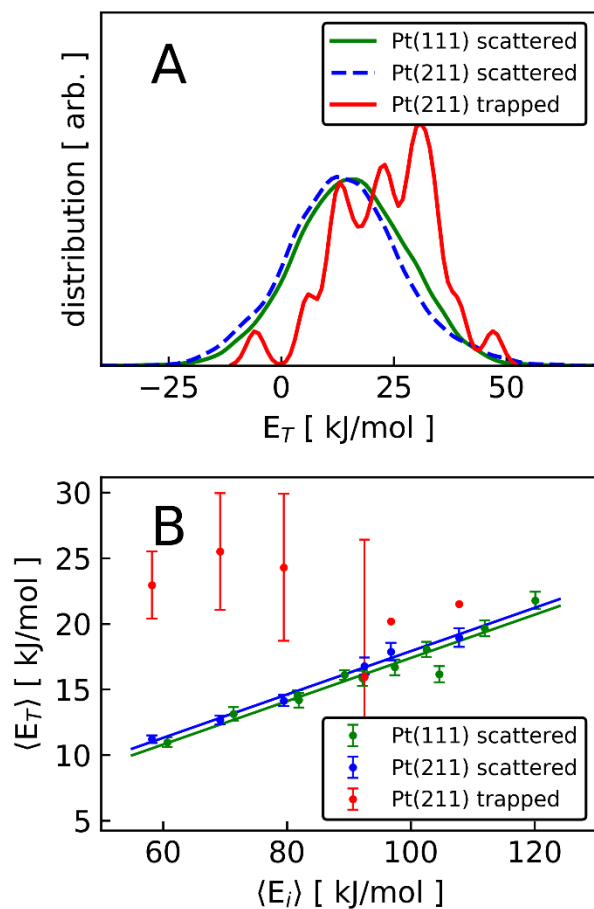
Figure 11. Panel A: energy transfer to the surface (E_T). Results are reported for scattered molecules on the flat Pt(111) (green line), on the stepped Pt(211) (blue line) and for trapped molecules (after the first impact on the Pt(211) (red line). Panel B: average energy transfer to the surface versus average incident energy ($\langle E_i \rangle$). Results are reported for scattered molecules on the flat Pt(111) (green), on the stepped Pt(211)) (blue) and for trapped molecules (after the first impact on the Pt(211)) (red). The lines are linear regressions of the data. Note that error bars are not shown for samples containing only one trapped trajectory.
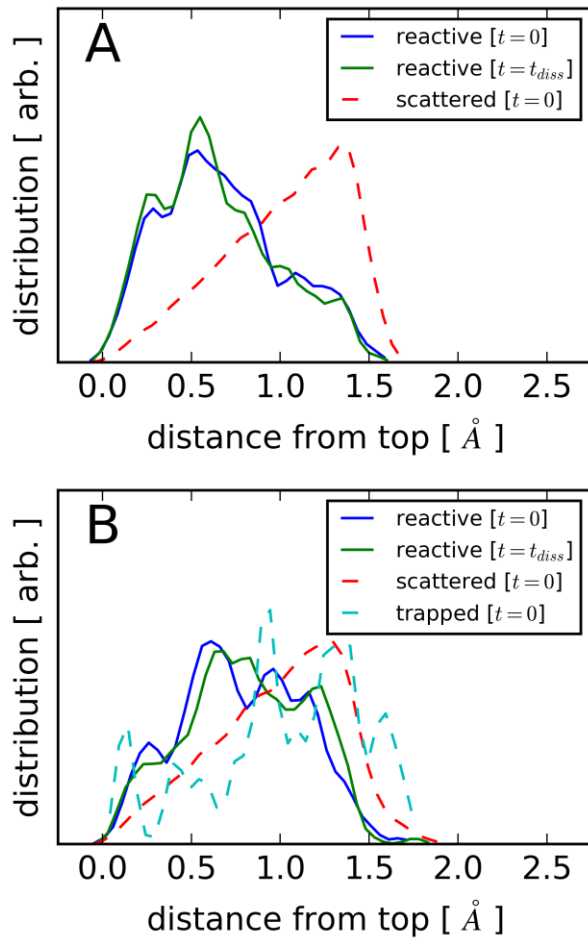
Figure 12. Distance from the closest top site in xy. In Panel A results for the Pt(111) surface and in Panel B for the Pt(211) surface are reported. Results for reactive trajectories are reported in blue and green for the initial position and the position at the dissociation time, respectively. Results for scattered and trapped trajectories are reported in red and cyan, respectively.
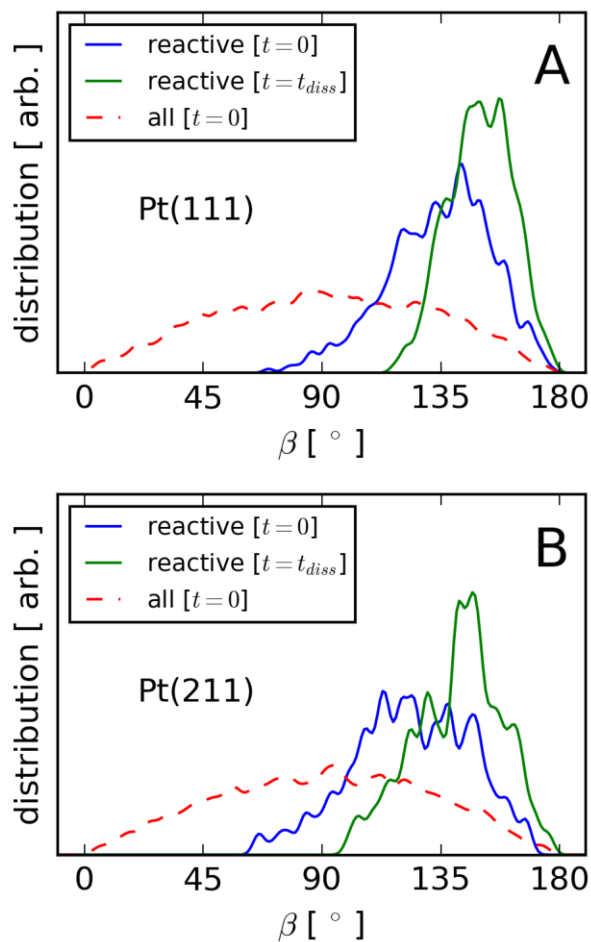
Figure 13. Panel A: β distributions for CHD$_3$ on Pt(111). Results for the reactive trajectories are reported in blue and green for the initial and the dissociation step, respectively. Results for the first time step of all the trajectories are reported in red. Panel B: same as Panel A but for Pt(211).
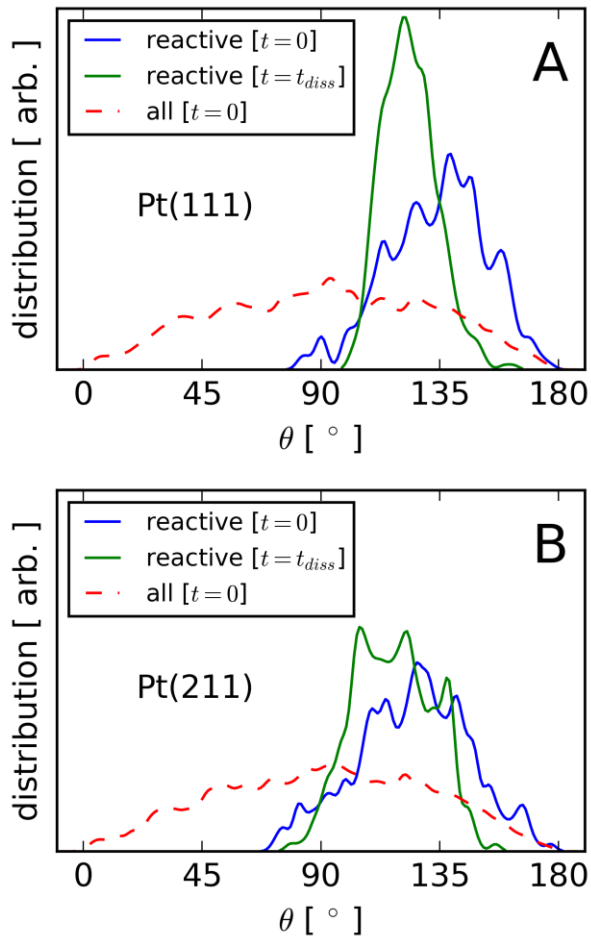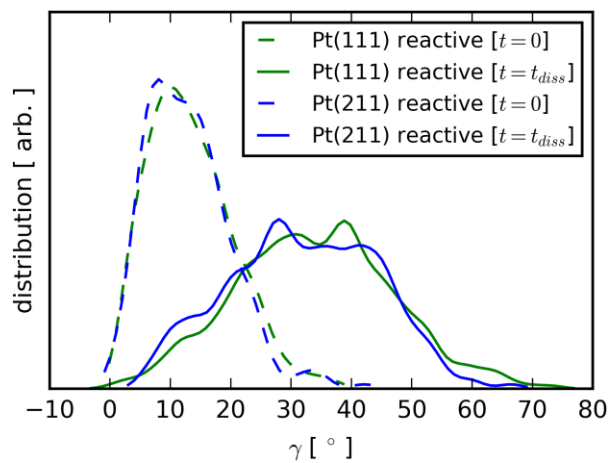
Figure 14. Same as Figure 13 but for θ.

Figure 15. γ distributions for t=0 and for the dissociation step as dashed and solid lines, respectively.

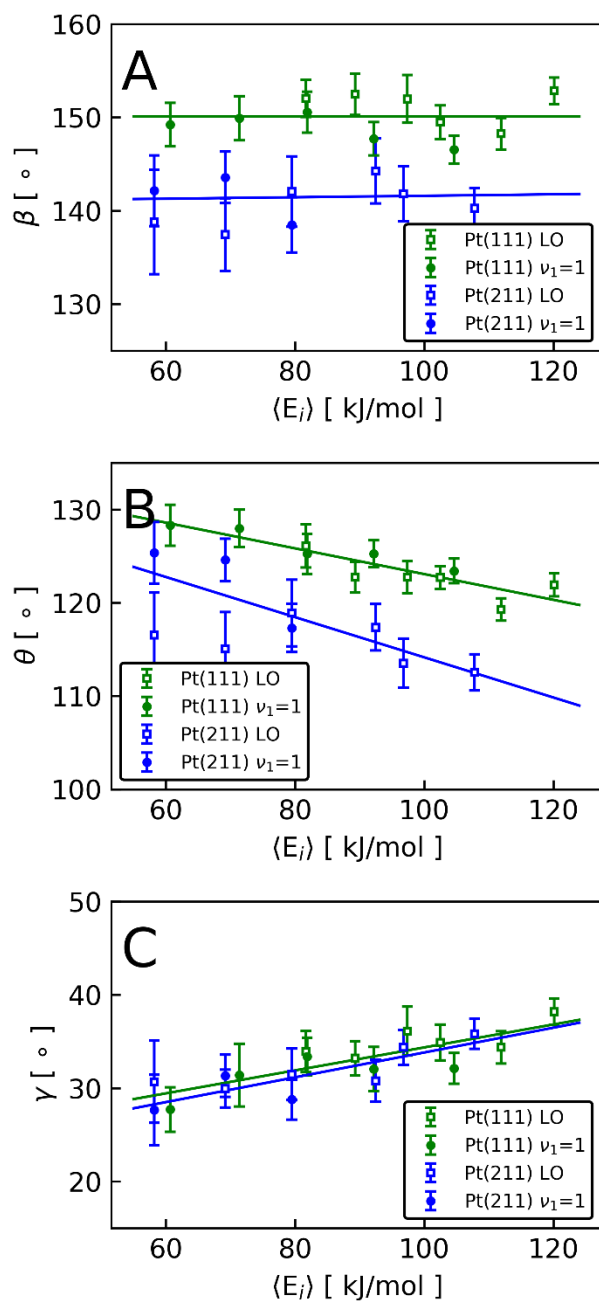Green lines are for Pt(111) and blue lines Pt(211) results.

Figure 16. Dependence of β, θ and γ on the initial average kinetic energy $\langle E_i \rangle$ at the moment of the dissociation. Results for the Pt(111) and for the Pt(211) are reported in green and blue, respectively. Open squares represent laser-off (LO) calculations and filled circles v_1=1 calculations. The linear regressions reported are computed considering both LO and v_1=1 trajectories.
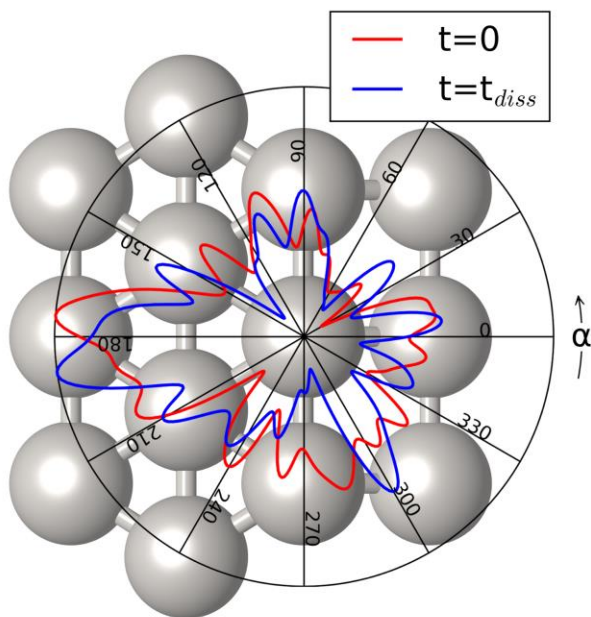
Figure 17. Distribution of α at t=0 and at the time of the dissociation (t_{diss}) (in red and blue, respectively) for molecules that reacted on the step edge atom. The value of α is reported in black and it increases counter-clockwise. The plot is superimposed on the Pt(211) 1st layer top view. The closer the distribution is to the external black circle the more that value of α is represented.

References

[1] C. A. Wolcott, A. J. Medford, F. Studt, and C. T. Campbell, J. Catal. **330**, 197 (2015).

[2] Y. Xu, A. C. Lausche, S. Wang, T. S. Khan, F. Abild-Pedersen, F. Studt, J. K. Nørskov, and T. Bligaard, New J. Phys. **15**, 125021 (2013).

[3] D. Migliorini, H. Chadwick, F. Nattino, A. Gutiérrez-González, E. Dombrowski, E. A. High, H. Guo, A. L. Utz, B. Jackson, R. D. Beck, and G. J. Kroes, J. Phys. Chem. Lett. **8**, 4177 (2017).

[4] G. Füchsel, P. S. Thomas, J. den Uyl, Y. Öztürk, F. Nattino, H. D. Meyer, and G. J. Kroes, Phys. Chem. Chem. Phys. **18**, 8174 (2016).

[5] F. Nattino, D. Migliorini, G. J. Kroes, E. Dombrowski, E. A. High, D. R. Killelea, and A. L. Utz, J. Phys. Chem. Lett. **7**, 2402 (2016).

[6] F. Nattino, D. Migliorini, M. Bonfanti, and G. J. Kroes, J. Chem. Phys. **144**, 044702 (2016).

[7] H. Guo and B. Jackson, J. Phys. Chem. C **119**, 14769 (2015).

[8] S. Nave and B. Jackson, Phys. Rev. Lett. **98**, 173003 (2007).

[9] A. K. Tiwari, S. Nave, and B. Jackson, J. Chem. Phys. **132**, 134702 (2010).

[10] X. Shen, Z. Zhang, and D. H. Zhang, J. Chem. Phys. **144**, 101101 (2016).

[11] R. R. Smith, D. R. Killelea, D. F. DelSesto, and A. L. Utz, Science **304**, 992 (2004).

[12] D. R. Killelea, V. L. Campbell, N. S. Shuman, and A. L. Utz, Science **319**, 790 (2008).

[13] R. D. Beck, P. Maroni, D. C. Papageorgopoulos, T. T. Dang, M. P. Schmid, T. R. Rizzo, Science **302**, 98 (2003).

[14] B. L. Yoder, R. Bisson, and R. D. Beck, Science **329**, 553 (2010).

[15] J. Wei and E. Iglesia, J. Phys. Chem. B **108**, 4094 (2004).

[16] B. Jiang, R. Liu, J. Li, D. Xie, M. Yang, and H. Guo, Chem. Sci. **4**, 3249 (2013).

[17] X. Shen, J. Chen, Z. Zhang, K. Shao, and D. H. Zhang, J. Chem. Phys. **143**, 144701 (2015).

[18] P. M. Hundt, B. Jiang, M. E. van Reijzen, H. Guo, and R. D. Beck, Science **344**, 504 (2014).

[19] S. Nave and B. Jackson, Phys. Rev. B - Condens. Matter Mater. Phys. **81**, 233408 (2010).

[20] B. Jackson and S. Nave, J. Chem. Phys. **138**, 174705 (2013).

[21] A. Farjamnia and B. Jackson, J. Chem. Phys. **142**, 234705 (2015).

[22] G. J. Kroes, J. Phys. Chem. Lett. **6**, 4106 (2015).

[23] C. Díaz, E. Pijper, R. A. Olsen, H. F. Busnengo, D. J. Auerbach, and G. J. Kroes, Science **326**, 832 (2009).

[24] L. Sementa, M. Wijzenbroek, B. J. van Kolck, M. F. Somers, A. Al-Halabi, H. F. Busnengo, R. A. Olsen, G. J. Kroes, M. Rutkowski, C. Thewes, N. F. Kleimeier, and H. Zacharias, J. Chem. Phys. **138**, 044708 (2013).

[25] E. Nour Ghassemi, M. Wijzenbroek, M. F. Somers, and G. J. Kroes, Chem. Phys. Lett. **683**, 329 (2017).

[26] Y. Y. Chuang, M. L. Radhakrishnan, P. L. Fast, C. J. Cramer, and D. G. Truhlar, J. Phys. Chem. A **103**, 4893 (1999).

[27] B. Hammer, L. B. Hansen, and J. K. Nørskov, Phys. Rev. B **59**, 7413 (1999).

[28] J. P. Perdew, K. Burke, and M. Ernzerhof, Phys. Rev. Lett. **77**, 3865 (1996).

[29] J. P. Perdew, K. Burke, and M. Ernzerhof, Phys. Rev. Lett. **78**, 1396 (1997).

[30] G. Román-Pérez and J. M. Soler, Phys. Rev. Lett. **103**, 096102 (2009).

[31] M. Dion, H. Rydberg, E. Schröder, D. C. Langreth, and B. I. Lundqvist, Phys. Rev. Lett. **92**, 246401 (2004).

[32] H. S. Taylor, Proc. R. Soc. London. Ser. A **108**, 105 (1925).

[33] T. Zambelli, J. Wintterlin, J. Trost, and G. Ertl, Science **273**, 1688 (1996).

[34] B. Hammer, Phys. Rev. Lett. **83**, 3681 (1999).

[35] A. T. Gee, B.E. Hayden, C. Mormiche, A. W. Kleyn, and B. Riedmüller, J. Chem. Phys. **118**, 3334 (2003).

[36] F. Abild-Pedersen, O. Lytken, J. Engbæk, G. Nielsen, I. Chorkendorff, and J. K. Nørskov, Surf. Sci. **590**, 127 (2005).

[37] G. Kresse and J. Hafner, Phys. Rev. B **49**, 14251 (1994).

[38] G. Kresse and J. Furthmüller, Phys. Rev. B **54**, 11169 (1996).

[39] G. Kresse and J. Furthmüller, Comput. Mater. Sci. **6**, 15 (1996).

[40] G. Kresse and J. Hafner, Phys. Rev. B **47**, 558 (1993).

[41] P. E. Blöchl, Phys. Rev. B **50**, 17953 (1994).

[42] G. Kresse and D. Joubert, Phys. Rev. B **59**, 1758 (1999).

[43] H. Chadwick, A. Gutiérrez-González, and R. D. Beck, J. Chem. Phys. **145**, 174707 (2016).

[44] P. Xiao, D. Sheppard, J. Rogal, and G. Henkelman, J. Chem. Phys. **140**, 174104 (2014).

[45] J. Kästner and P. Sherwood, J. Chem. Phys. **128**, 014106 (2008).

[46] A. Heyden, A. T. Bell, and F. J. Keil, J. Chem. Phys. **123**, 224101 (2005).

[47] G. Henkelman and H. Jónsson, J. Chem. Phys. **111**, 7010 (1999).

[48] S. Nave, A.K. Tiwari, and B. Jackson, J. Chem. Phys. **132**, 054705 (2010).